NEOPLASIA
www.neoplasia.com

Volume 22 Number 10 October 2020 pp. 470–483

Real-time sensing of MAPK signaling in medulloblastoma cells reveals cellular evasion mechanism counteracting dasatinib blockade of ERK activation during invasion

Marc Thomas SchÎnholzer [a]; Jessica Migliavacca [a]; Elena Alvarez [a]; Karthiga Santhana Kumar [a]; Anuja Neve [a]; Alexandre Gries [a]; Min Ma [b]; Michael A. Grotzer [a,c]; Martin Baumgartner [a,*]

[a] Pediatric Neuro-Oncology Research Group, University Children's Hospital ZÍrich, Children's Research Center, Balgrist Campus, Lengghalde 5, CH-8008 ZÍrich, Switzerland; [b] Quantitative Signaling Group, Department of Fundamental Microbiology, University of Lausanne, CH-1015 Lausanne, Switzerland; [c] University Children's Hospital ZÍrich, Steinwiesstrasse 75, CH-8032 ZÍrich, Switzerland

Abstract

Aberrantly activated kinase signaling pathways drive invasion and dissemination in medulloblastoma (MB). A majority of tumor-promoting kinase signaling pathways feed into the mitogen-activated protein kinase (MAPK) extracellular regulated kinase (ERK1/2) pathway. The activation status of ERK1/2 during invasion of MB cells is not known and its implication in invasion control unclear.

We established a synthetic kinase activation relocation sensor (SKARS) for the MAPK ERK1/2 pathway in MB cells for real-time measuring of drug response. We used 3D invasion assays and organotypic cerebellum slice culture to test drug effects in a physiologically relevant tissue environment.

We found that hepatocyte growth factor (HGF), epidermal growth factor (EGF), or basic fibroblast growth factor (bFGF) caused rapid nuclear ERK1/2 activation in MB cells, which persisted for several hours. Concomitant treatment with the BCR/ABL kinase inhibitor dasatinib completely repressed nuclear ERK1/2 activity induced by HGF and EGF but not by bFGF. Increased nuclear ERK1/2 activity correlated positively with speed of invasion. Dasatinib blocked ERK-associated invasion in the majority of cells, but we also observed fast-invading cells with low ERK1/2 activity. These ERK1/2-low, fast-moving cells displayed a rounded morphology, while ERK-high fast-moving cells displayed a mesenchymal morphology. Dasatinib effectively blocked EGF-induced proliferation while it only moderately repressed tissue invasion, indicating that a subset of cells may evade invasion repression by dasatinib through non-mesenchymal motility. Thus, growth factor-induced nuclear activation of ERK1/2 is associated with mesenchymal motility and proliferation in MB cells and can be blocked with the BCR/ABL kinase inhibitor dasatinib.

Neoplasia (2020) 22 470–483

Keywords: Medulloblastoma, Nuclear ERK1/2 activation sensor, Cell migration, Cerebellum slice culture, Fluorescent biosensor, Live cell imaging

Introduction

The mitogen-activated protein kinase (MAPK) signaling pathways are evolutionary conserved signaling modules leading to the activation of either extracellular regulated kinases (ERKs), p38 activated kinase or c-jun N-terminal kinase (JNK). MAPK signaling is induced by extracellular cues and transmitted through a tier of sequentially activated receptors, adaptor proteins, small GTPases and kinases that control differentiation, proliferation, viability and migration of cells and tissues. Aberrant activation of MAPK signaling, for example by the amplification of a pathway-inducing receptor, by the mutational alterations of receptors or signal-transmitting intermediates or by the inactivation of pathway repressors is observed in multiple tumors including medulloblastoma (MB) [1–6],

Abbreviations: bFGF, basic fibroblast growth factor, c-Met, cellular mesenchymal epithelial transition factor, EGF, epidermal growth factor, ERK, Extracellular regulated kinase, FDA, food and drug administration, FGFR, fibroblast growth factor receptor, HGF, hepatocyte growth factor, JNK, c-jun N-terminal kinase, MAPK, mitogen-activated protein kinases, MB, medulloblastoma, SHH, sonic hedgehog, SKARS, Synthetic Kinase Activation Relocation Sensor, WST, water soluble tetrazolium salt

* Corresponding author.
e-mail address: Martin.Baumgartner@kispi.uzh.ch (M. Baumgartner).

https://doi.org/10.1016/j.neo.2020.07.006

the most common malignant brain tumor in children. Molecular profiling of MB defined four subgroups with a total of 12 subtypes [7,8], with variable demographic, clinical and molecular features [9]. The large heterogeneity of MB tumors underscores the necessity to identify those MB tumors potentially susceptible to MAPK-ERK1/2 inhibition. With CD271 [2] and BMI1 [10] two such biomarkers were identified for sonic hedgehog (SHH) and Group 4 (Gr4) MB tumors [9], respectively.

The regulated translocation of activated ERK1/2 into the nucleus thereby constitutes a particular function of the pathway, as it causes the spatial separation of the activated kinase and the phosphorylation of a selected repertoire of substrates [11]. The C-terminal region and in particular amino acids Asp-316, Asp-319 and Glu-320 were found to be required for nuclear translocation [12], which is mediated by the phosphorylation-dependent release of the cytosolic anchoring protein and shuttling via importin 7 [13,14]. The nuclear activation of ERK1/2 in cells and tissues and the functional significance of spatio-temporal activation for normal and aberrant cell function are incompletely understood. With new tools for real-time visualization of nuclear ERK1/2 activities established, including ERK1/2-nKTR, a genetically encoded biosensor for extracellular regulated kinase [15], ERK1/2 activation patterns can now be tracked and correlated with cellular functions. This sensor was further developed and adapted to the mammalian system for quantifying MAPK dynamics in living mammalian cells [16].

Direct repression of MAPKs MEK or ERK1/2 or the upstream activator Ras are associated with the emergence of resistance either by the reactivation of ERK1/2 through impaired repression or the activation of an alternative pathway [17–19]. One potential indirect repressor of ERK1/2 activation in tumor cells is dasatinib, a second-generation multitarget kinase inhibitor targeting both SRC and BCR-ABL kinases. It was discovered as a small molecular inhibitor binding to ABL with less stringent conformational requirements than Imatinib and shown to effectively inhibit BCR/ABL-driven diseases [20]. Dasatinib is FDA-approved for the treatment of chronic myeloid leukemia that is resistant to imatinib treatment. Aberrant receptor tyrosine kinase (RTK) and SRC kinase signaling are hallmarks of Gr4 medulloblastoma [21] and the activation of c-MET [22–24] or FGFR [25] promotes migration and invasion in SHH and Gr4 MB tumor cells. EGF signals through HER2 and EGFR and blockade of these receptors by gefitinib reduces MB tumor growth and invasion [6]. SRC is a downstream effector of these signaling pathways, and it was suggested that dasatinib could be an effective inhibitor of RTK-driven MB pathologies [21]. Indeed, an earlier study already described inhibitory effects of dasatinib alone or in synergy with the aurora kinase inhibitor AT9283 on cell migration and proliferation [26]. More recently, a combinatorial effect on MB tumor cell clonogenicity was observed after treatments with dasatinib and cisplatin [27]. The aims of this study were to test the efficacy of FDA-approved drugs in repressing HGF-induced invasion of SHH MB cells, to monitor nuclear MAPK signaling in response to growth factors in real-time and to determine whether drug repression of invasiveness correlates with decreased nuclear MAPK activity.

Material and methods

Cell lines and reagents

The DAOY cell line was obtained from ATCC (HTB-186, authenticated: June 15, 2018) and cultured in IMEM (A1048901, Thermo Fisher, Waltham, MA, USA) as described in [28]. ONS-76 [29] were kindly provided by Xiaochong Wu, The SickKids, Toronto, and cultured in DMEM. The culture medium was supplemented with FBS (10%) and penicillin/streptomycin (1%). Serum-free medium (SFM) is IMEM, supplemented with penicillin/streptomycin (1%). The pMM55_pLV-CMV-MEK2-2NLS-mClover plasmid [16] for CMV-driven ERK Synthetic Kinase Activation Relocation Sensor (ESKARS) expression was provided by M. Ma. Infectious lentiviral particles of rLV.EF1.mCherry-Nuc-9 for nuclear expression of mCherry were purchased from Takara Bio Inc. (Kusatsu, Japan). Stable ESKARS and m-Cherry-nuc expressing DAOY cells were generated by lentiviral transduction. ESKARS encoding VSVG-coated lentivirus was generated by transfection of HEK-293T cells with the lentiviral packaging vectors pPax2, pVSVG and pMM55_pLV-CMV-MEK2-2NLS-mClover (4.5:3.0:7.5). Virus supernatant was harvested 30 h after transfection and target cells were transduced in the presence of polybrene (1:1,000). Stable cell lines were selected with puromycin [2 µg/ml] (rLV.EF1.mCherry-Nuc-9) or blasticidin [4 µg/ml] (pMM55_pLV-CMV-MEK2-2NLS-mClover). DAOY LA-EGFP cells were produced by lentiviral transduction of DAOY cells with pLenti-LA-EGFP [24].

Growth factors, drugs and concentrations used

HGF: 20 ng/ml, EGF: 30 ng/ml, bFGF: 100 ng/ml (all from Preprotech). Drugs: (all from Selleckchem, Pittsburg, PA, USA): SCH772984: 1 µM, Staurosporin: 1 µM, H_2O_2: 800 mM. Axitinib: 1 µM, 5 µM, 10 µM, NPV-BEZ35: 250 nM, 500 nM, 1 µM, 5 µM, 10 µM, dasatinib (BMS-354825): 250 nM, 1 µM, 5 µM, 10 µM, Erlotinib HCI: 250 nM, 500 nM, 1 µM, 5 µM, 10 µM, Imatinib mesylate: 1 µM, 5 µM, 10 µM, Nilotinib (AMN-107): 1 µM, 5 µM, 10 µM, Rapamycin (sirolimus): 250 nM, 500 nM, 1 µM, 5 µM, 10 µM, Sunitinib malate (sutent): 1 µM, 5 µM, 10 µM, Temsirolimus (torisel): 1 µM, 5 µM, 10 µM, Masitinib (AB1010): 500 nM, 1 µM, 5 µM, 10 µM, Crizotinib (PF-02341066): 250 nM, 500 nM, 1 µM, 5 µM, 10 µM, Foretinib: 500 nM, 1 µM, 5 µM, 10 µM (Selleckchem), XL-184: 1 µM, 5 µM, 10 µM, Vermurafenib (PLX4032): 1 µM, 5 µM, 10 µM, Zoledronic acid (zoledronate): 1 µM, 5 µM, 10 µM, Ruxolitinib (INCB018424): 500 nM, 1 µM, 5 µM, 10 µM, Nystatin (mycostatin): 1 µM, 5 µM, 10 µM, lapatinib: 1 µM, 5 µM, 10 µM, Pazopanib: 1 µM, 5 µM, 10 µM, dequalinium chloride: 1 µM, 5 µM, 10 µM, Tofacitinib citrate (CP-690550 citrate): 500 nM, 1 µM, 5 µM, 10 µM. H-1152 (from Alexis Biochemicals): 1 µM.

Spheroid invasion assay (SIA)

SIA was performed and quantified according to [30]. In brief: 2,000 cells were seeded in 100 µl complete medium per well in cell-repellent 96 well microplates (650790, Greiner Bio-One, KremsmĬnster, Austria). Cells were allowed to form spheroids for 24 h after which 70 µl medium were removed and replaced with 70 µl of a mixture containing 3.65 µl sodium bicarbonate (7.5%), 6.64 µl 10× DMEM and 59.71 µl PureCol (3 mg/ml, CellSystems, Troisdorf, Germany). Polymerized collagen I hydrogels were overlaid with 100 µl SFM containing growth factors and inhibitors. Growth factor stimulation were performed with bFGF (100 ng/ml), HGF (20 ng/ml) or EGF (30 ng/ml). Growth factors and drugs were mixed in 2× concentration into the 100 µl SFM to reach 1× concentration in the final dilution. Cell dissemination was acquired 24 h post treatment with an AxioObserver wide-field microscope using a 5× objective (Zeiss, Jena, Germany) and analyzed with our in-house cell dissemination counter software aSDICs [30]. This software determines the distance of each nucleus of the migrating cells to the center of the spheroid. Mean distance and total cumulated distance of invasion is quantified.

Confocal microscopy analysis of spheroids in collagen I

Tumor cell spheroids were grown as described above for the SIA. Glass bottom 96 well plates (Cellvis, P96-1.5H-N) were made low adhesive using Lipidure (0.5% in EtOH, 20 µl of a 5 mg/ml solution per well). Plate with Lipidure was placed on a horizontal shaker for 10 min and then

maintained at room temperature until EtOH was evaporated. Spheroids were transferred into these pretreated plates and embedded in collagen I. Spheroids were left untreated or treated with the following conditions: EGF 30 ng/ml, dasatinib 250 nM, H-1152 1 μM, EGF + dasatinib, EGF + H-1152, EGF + dasatinib + H-1152. After 16 h, cells were fixed in 4% PFA and nuclei labeled with Hoechst 33342, 1:5000 dilution. Images were acquired with a 20× immersion objective on a Leica SP8 confocal microscope. 1024 × 1024 pixels image stacks with 1 μm Z-distance from the whole spheroid or single cells were acquired.

Cell-Tox green cytotoxicity assay

i96 well plates

2500 ONS-76 cells were seeded in 100 μl per well of complete RPMI medium in 96-well low adhesion plate (Greiner bio-one, 650970, Germany) for 24 h to form spheroids. After spheroid formation, 50 μl of medium per well were removed and replaced by 50 μl fresh medium containing increasing concentrations of drugs, complemented with 1:500 of CellTox™ Green Dye (G8742, Promega) as described by the manufacturer. The fluorescence levels representing the nonviable cell population were measured after 24, 48 and 72 h using a Cytation 3 imaging reader BioTek® (λ_{ex} = 485 nm, λ_{em} = 520 nm). The cytotoxicity curve was generated with GraphPad Prism 8 software as log (inhibitor) vs. response – Variable slope (four parameters) with 100% as the effect observed with the highest concentration of dasatinib (80 μM).

i384 well plates

250 DAOY cells in 20 μl per well were seeded in a 384 well Corning spheroid microplate (Corning Incorporated, NY, USA). After 24–48 h, FDA-approved drugs were dispensed with a hp d300 digital dispenser in three different concentrations. Staurosporin (250 nM, 500 nM, 1 μM and 2 μM) and H_2O_2 (800 mM) were used as positive controls. After 24 h, cell tox green was added (20 μl per well). After an incubation time of 15 min at room temperature and protected from light, the fluorescence signal was measured using a Cytation 3 imaging reader BioTek® (λ_{ex} = 485 nm, λ_{em} = 520 nm.

WST-1 cell proliferation assay, DAOY cells

1,000 cells were seeded in 100 μl complete IMEM in 96-well plates (Greiner μClear). Wells lining the borders of the plate were filled with PBS. The plates were incubated for 24, 48, 72, or 96 h. After addition of 10 μl WST-1 (Roche Diagnostics) reagent, cells were incubated at 37 °C for 30 min before absorbance was measured at 440 nm using a microplate reader. Medium containing GFs and inhibitors was changed daily. For each condition, a blank measurement pas performed for background subtraction. Data analysis was performed using GraphPad Prism 7.

ESKARS analysis two-dimensional (2D) system

5,000 cells were seeded in a 96-well plate (Greiner μClear) in 100 μl complete medium. After 6 h, the complete medium was replaced with starvation medium and cells were incubated overnight at 37 °C. After starvation, growth factors and inhibitors were added individually, and plates sealed with a gas-permeable membrane. Image acquisition was started 1 min after treatment using a Molecular Devices ImageXpress^{MICRO} equipped with a 20× objective and a climate chamber with temperature and CO_2 control. Cells were imaged with an exposure time of 25–35 ms, using either the 531 nm (mCherry-nuc-9) or 482 nm (ESKARS) wavelengths. The interval time between acquisitions was 60 s and duration of image acquisition between 5 and 240 min. Video files were converted into image sequences using ImageJ (version 1.51 g) and channels separated into gray-scale images using CellProfiler (version 2.2.0). Nuclei were identified using the mCherry-nuc-9 fluorescence and defined as primary objects. Primary objects outside the set diameter range of 40–80 pixels or touching an edge of the image were excluded. Primary objects were used as masks to mark the nuclear boundaries and to track single cells. The maximum gap distance between objects per interval was set to 50 pixels. Pixel intensities in the cytoplasmic compartment were quantified by expanding the primary objects by 70 pixels, which resulted in a circular mask surrounding the primary object. This mask was applied to the green channel (ESKARS fluorescence) for the quantification of the cytoplasmic pixel intensities. Data processing and visualization were performed in R and GraphPad Prism 7, respectively.

ESKARS analysis in three-dimensional (3D) matrix

Spheroids were generated as described for the SIA. Single spheroids were transferred in 9 μl medium into separate wells of 15-well Angiogenesis slides (ibidi, Martinsried, Germany). Subsequently, 21 μl of a 2.5% PureCol solution was added to each well. After polymerization at 37 °C, growth factors and inhibitors were added dropwise to the wells. The images were acquired using a CLSM-Leica SP8 confocal microscope equipped with temperature- and CO_2-controlled stage and a 10× objective. Total acquisition time was 24 h with time intervals of 10 min. Format 1024 × 1024, speed 8000 (with resonant scanner), bidirectional on, zoom factor 1.7, line average 64, number of steps: 15, Z-step size 5.0 μm.

The exported video files were further processed using Imaris (version 9.2.0). mCherry-nuc-9 fluorescence was determined as a mask for delineating the area of the nuclei and used to measure the mean intensity of the ESKARS fluorescence within the nucleus. Digital thresholding was performed using Imaris. The background was subtracted at the value of 23.8112 and the diameter of the largest sphere was determined as 5.02 μm. The surface grain size was set to 1.34 μm and only objects containing more than 100 voxels were included. Autoregressive motion was applied for nuclei tracking with the maximal distance covered between two intervals set to 14.5 μm. The maximal gap size was defined as 3 and the filling of gaps was enabled. For the analysis, only tracks with a duration longer than 2000 s were included

Single cell motility analysis

5000 cells DAOY-LA-EGFP per well in 200 μl medium with 1.5% FBS were seeded on collagen IV-coated 8-well slides (ibidi, Martinsried, Germany). After 4 h, EGF (30 ng/ml) or bFGF (100 ng/ml) or EGF + 250 nM dasatinib or bFGF + 250 nM dasatinib were added in 100 μl SFM (final FBS concentration: 1%). Time-lapse imaging was performed with a widefield Nikon Eclipse Ti2 inverted microscope equipped with temperature and CO_2-controlled stage incubation system. Images were recorded in EGFP channel using a 20× dry objective in 15 min intervals. Total acquisition time was 18 h. Images were assembled in .avi movie and analyzed in Fiji (ImageJ [31]). .avi movies were converted to gray scale and brightness/contrast adjusted so that also weakly LA-EGFP-positive cells were detected. Images were thresholded and threshold applied to whole image stack. Images were then converted into binary images. Tracking was performed using the MtTrack2 plugin (Object size: 60, max object size: 800, maximum velocity: 100, minimum track length: 50). Speed in μm/min and directionality (displacement:path length) was calculated for all recorded cells and plotted as violin plots in prism.

Data rearrangement and statistical analysis

The rearrangement of the different data sets was performed using R (versions 3.5.1 and 3.5.2) and RStudio (version 0.99.903). Statistical analysis was performed using GraphPad Prism (versions 7 and 8).

Ex vivo organotypic cerebellum slice culture (OCSC)

Cerebellar slices were prepared form P8-10 C57BL/6JRj mouse pups as described in [32]. Slices were kept in culture for 15 days, during which we monitored sliced for signs of apoptosis. We changed the media daily. Tumor spheroids were formed with DAOY LA-EGFP cells. The co-culture was treated with EGF (30 ng/ml), dasatinib (250 nM) or the combination of the two treatments. Spheroids were incubated for 5 days. Following the treatment, the co-cultures were fixed and stained as described in [32] and analyzed using confocal immunofluorescence microscopy.

Results

Dasatinib blocks collagen invasion and proliferation of SHH MB cell lines

In a search for FDA-approved kinase inhibitors (Fig. 1A) that repress growth factor-induced collagen I invasion, we identified dasatinib as an effective inhibitor of HGF-induced invasion in DAOY MB cells (Fig. 1B). This effect of dasatinib was not the result of cytotoxicity, as we observed no increase in cell death in cells treated with up to 10 μM (Fig. 1C and 2C). To determine whether dasatinib also blocks invasion induced by bFGF or EGF, we quantified growth factor-induced collagen I invasion of tumor cell spheroids [30] in the presence of dasatinib (Fig. 2A). Dasatinib effectively blocked collagen I invasion driven by the three growth factors with an IC_{50} ranging from 9.44 nM (bFGF) to 38.28 nM (HGF) to 71.78 nM (EGF, Fig. 2B). Basal collagen I invasion in the absence of growth factor stimulation was also blocked with a moderately higher EC50 of 110.40 nM. Dasatinib and danusertib, another BCR-ABL/SRC inhibitor, but not erlotinib, an EGFR inhibitor, effectively blocked collagen I invasion of ONS-76, a SHH MB line that invades collagen I gels under low serum condition independent of growth factor stimulation (Fig. 2C). We calculated the IC_{50} of dasatinib in ONS-76 cells as 3.95 nM and observed cytotoxicity only well above 10 μM drug concentration (Fig. 2C). Dasatinib also markedly reduced the speed of EGF- or bFGF-induced single cells migrating on collagen IV coated slides, although a remarkable number of cells still migrated in the presence of dasatinib (Fig. S1, M1 – M5). In the 3D migration analysis, 250 (bFGF), 500 (HGF) or 1000 (EGF) nM dasatinib was necessary to reduce growth factor-induced collagen I invasion to baseline (Fig. S2). To determine the impact of dasatinib treatment on proliferation and viability in DAOY cells, we performed a WST-1 assay with increasing concentrations of dasatinib in regular growth medium. No significant repression of proliferation was observed up to 24 h of treatment for all concentrations tested. Exposure to inhibitor concentrations up to 125 nM for 48 h caused marked repression of proliferation, and concentrations of 250 nM or higher almost completely abrogated proliferation (Fig. 2D). These data indicate that migration and proliferation of MB cells can be effectively blocked by dasatinib at nanomolar to low micromolar concentrations without the implication of cytotoxicity.

Dasatinib prevents nuclear ERK1/2 activity induced by growth factor stimulation

The activation of the MAPK pathway is a hallmark signature of receptor tyrosine kinase activation. The effector kinases of this layered signaling pathway are the extracellular regulated kinases ERK1/2, p38 and JNKs. Nuclear translocation of ERK1/2 is necessary for controlling nuclear substrates and is associated with oncogenesis (reviewed in [11]). To determine nuclear translocation dynamics of activated ERK1/2 in real time in living MB cells, we established the SKARS [16] biosensor for ERK1/2 in DAOY MB cells (DAOY-ESKARS, Fig. S3). To test sensor functionality, we stimulated DAOY-ESKARS cells with EGF and monitored translocation of the biosensor. Nuclear fluorescence – indicative for lack of nuclear ERK1/2 activity – was observed in starved cells. EGF stimulation caused rapid translocation of the sensor to the cytoplasm, with a concomitant increase of the cytoplasm:nucleus ratio (Fig. 3A). We tested the effect of EGF, HGF and bFGF on sensor translocation over a period of 2 h. As a control for specific translocation repression, we treated the cells with the ERK1/2 inhibitor SCH772984. We found that all three growth factors caused rapid and sustained sensor translocation, which indicates nuclear ERK1/2 activation (Fig. 3B). Pharmacological inhibition of ERK1/2 kinase activity abrogated sensor translocation, thus confirming that latter depends on active ERK1/2. ERK1/2 sensor activity returns rapidly to baseline after GF wash-out and remains low in the presence of SCH772984, demonstrating that sensor response is fast and reversible. To test whether dasatinib can block growth factor induced nuclear ERK1/2 activity, we compared cytoplasm:nucleus ratio in cells treated with the growth factors or with growth factors in combination with dasatinib. HGF- and EGF-induced nuclear ERK1/2 activity started to decrease and reached baseline within 1 h of dasatinib treatment and remained at baseline levels for the whole observation period of 3.5 h (Fig. 3C). In contrast, bFGF-induced nuclear ERK1/2 activity was only moderately repressed and repression did not reach baseline levels throughout the whole observation period. These data show that HGF- and EGF-induced nuclear ERK1/2 activation is completely repressed by dasatinib, whereas bFGF-induced nuclear ERK1/2 activation is incompletely repressed and thus partially independent of the kinases inhibited by dasatinib.

ERK1/2 is active in the nucleus of invading cells

Although pharmacological or genetic inhibition of ERK1/2 repressed growth factor-induced collagen I invasion [25], it is not known whether invasion correlates positively with increased nuclear ERK1/2 activity. To test whether nuclear ERK1/2 activity could be required for invasive motility, we determined the ratio of nuclear to cytoplasmatic ESKARS fluorescence in cells invading the collagen I matrix. Within ten hours, we observed invasive protrusions and invading cells in unstimulated cells in serum-free medium (Fig. 4A, M6). Dasatinib treatment under these conditions completely blocked invasion and invasive protrusion (M7). In addition, we observed the appearance of cell debris in the immediate vicinity of the spheroid (Fig. 4A, arrowheads), indicative for cell death. EGF stimulation triggered massive collagen I invasion (Fig. 4B, left, M8), which was largely but not completely blocked by dasatinib treatment (Fig. 4B, right, M9). In contrast to dasatinib-treated control spheroids without serum or growth factor (M7), we observed no cellular debris in dasatinib-treated spheroids co-stimulated with EGF (M9). HGF (M10) and bFGF (M12) also induced massive collagen I invasion whereby the pattern of HGF-induced invasion is different (Fig. 4A), with overall fewer invading cells and proportionally more cells invading as single cells with no evident cell–cell contact. In the presence of dasatinib, neither HGF (M11) nor bFGF (M13) stimulation did prevent the appearance of cell debris (Fig. 4A). Using ESKARS, we quantified nuclear ERK1/2 activity in the cells during collagen I invasion, to determine whether speed of migration in collagen I correlated positively with nuclear ERK1/2 activity. To do that, we grouped the cells according to speed in slow (low 25 percentile), intermediate (interquartile range) and fast (top 25 percentile) moving cells

A

Name	Concentration	Target
Crizotinib	250 nM, 1 μM	c-Met
XL-184 (Cabozantinib)	1 μM, 10 μM	c-Met
Erlotinib HCl	1 μM	EGFR
Vemurafenib	1 μM, 5 μM	B-Raf
Ruxolitinib	1 μM, 5 μM	JAK
Tofacitinib citrate	1 μM, 5 μM	JAK
Rapamycin (Sirolimus)	500 nM, 1 μM	mTOR
Temsirolimus (Torisel)	1 μM	mTOR
Dasatinib	1 μM	Src, Bcr-Abl, c-Kit
Nystatin (Mycostatin)	1 μM, 10 μM	PI3K, Akt, mTOR
Zoledronic Acid (Zoledronate)	5 μM, 10 μM	PKC
Dequalinium chloride	1 μM	PKC

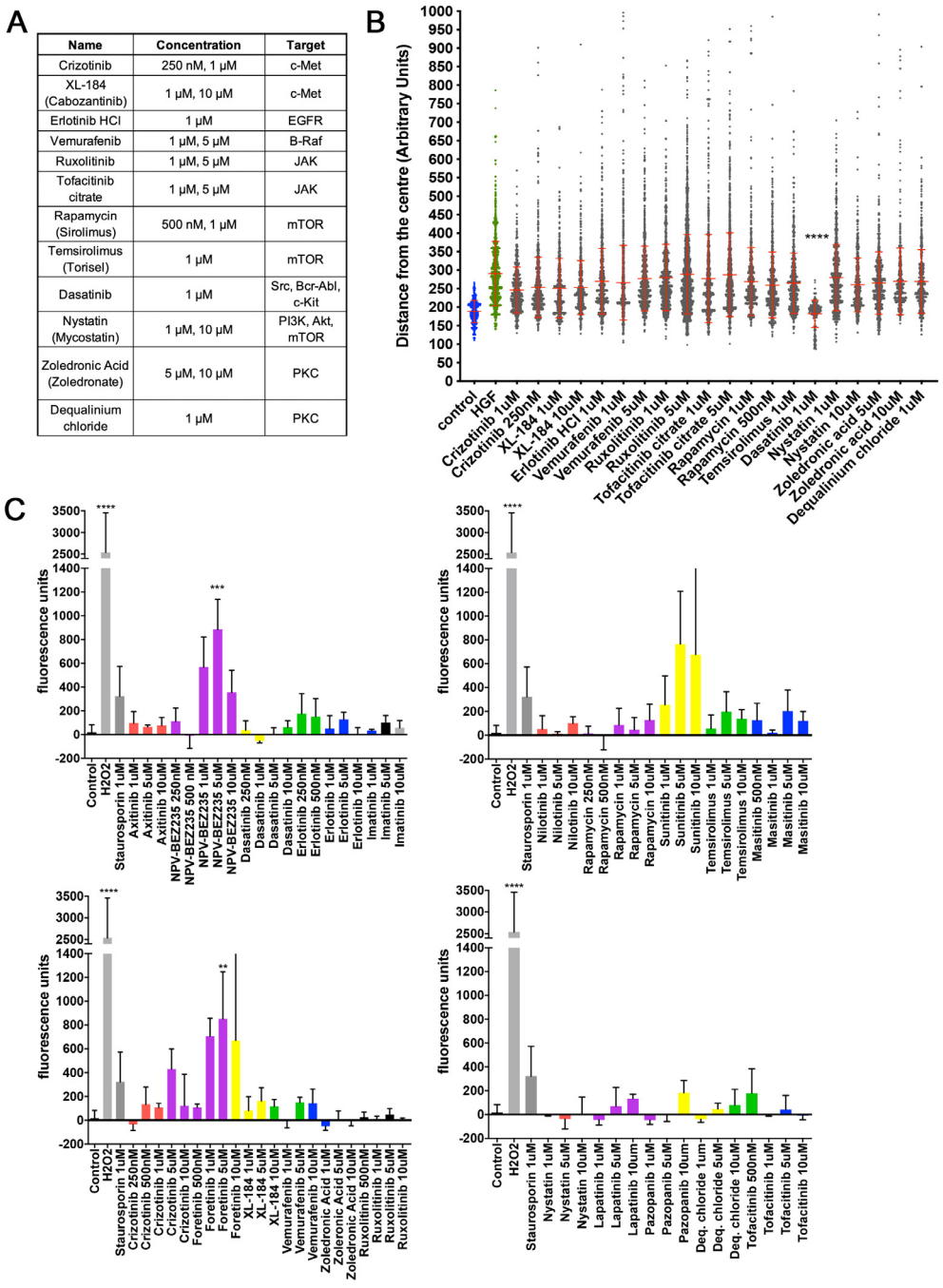

Fig. 1. Identification of dasatinib as a non-toxic invasion inhibitor. (A) List of FDA-approved kinase inhibitors, concentrations used and predicted targets. (B) Spheroid invasion assay (SIA) comparing the inhibitory effects of the kinase inhibitors at the indicated concentrations in the presence of HGF. Each dot represents the distance in pixel of a single cell from the center of the spheroid. (C) CellTox green cytotoxicity assay to test the viability of tumor cell spheroids exposed to the indicated concentrations of drugs for 24 h. H_2O_2 and staurosporin were used as positive controls.

(Fig. 5A). We then determined the nuclear ERK1/2 activity based on the levels of nuclear ESKARS fluorescence, whereby low mean pixel intensity indicates high ERK1/2 activity (Fig. 5B). We performed this for all migrating cells in the absence and presence of growth factors (bFGF, HGF or EGF) and without or with dasatinib (Fig. 5C, S4A). We observed that fast-moving cells generally displayed a decreased, and slow-moving cells an increased nuclear ESKARS fluorescence intensity. This indicated that cell speed in the three-dimensional collagen matrix correlates positively with nuclear ERK1/2 activity (Fig. 5C, S4A). Dasatinib treatment reduced the total number of migrating cells (Fig. 4A). The majority of the remaining fast-moving cells still displaced high nuclear ERK1/2 activity (Fig. 5C, S4A). However, some very fast-moving cells displayed pronounced nuclear ESKARS fluorescence, indicative of very low nuclear ERK1/2 activity. bFGF or EGF stimulation significantly increased the percentage of fast-moving cells with low nuclear ERK activity (Fig. 5D). The fast-moving, low nuclear ERK1/2 cells migrated less directionally (Fig. S4B) and displayed a rounded morphology (M9), contrasting with the mesenchymal, elongated morphology observed in control cells. Thus, growth factor stimulation triggers nuclear ERK1/2 activity, which is associated with increased migration inside the 3D collagen I matrix. Dasatinib represses nuclear ERK1/2 activation and significantly reduces 3D migration. Activated growth factor signaling in the presence of dasatinib also

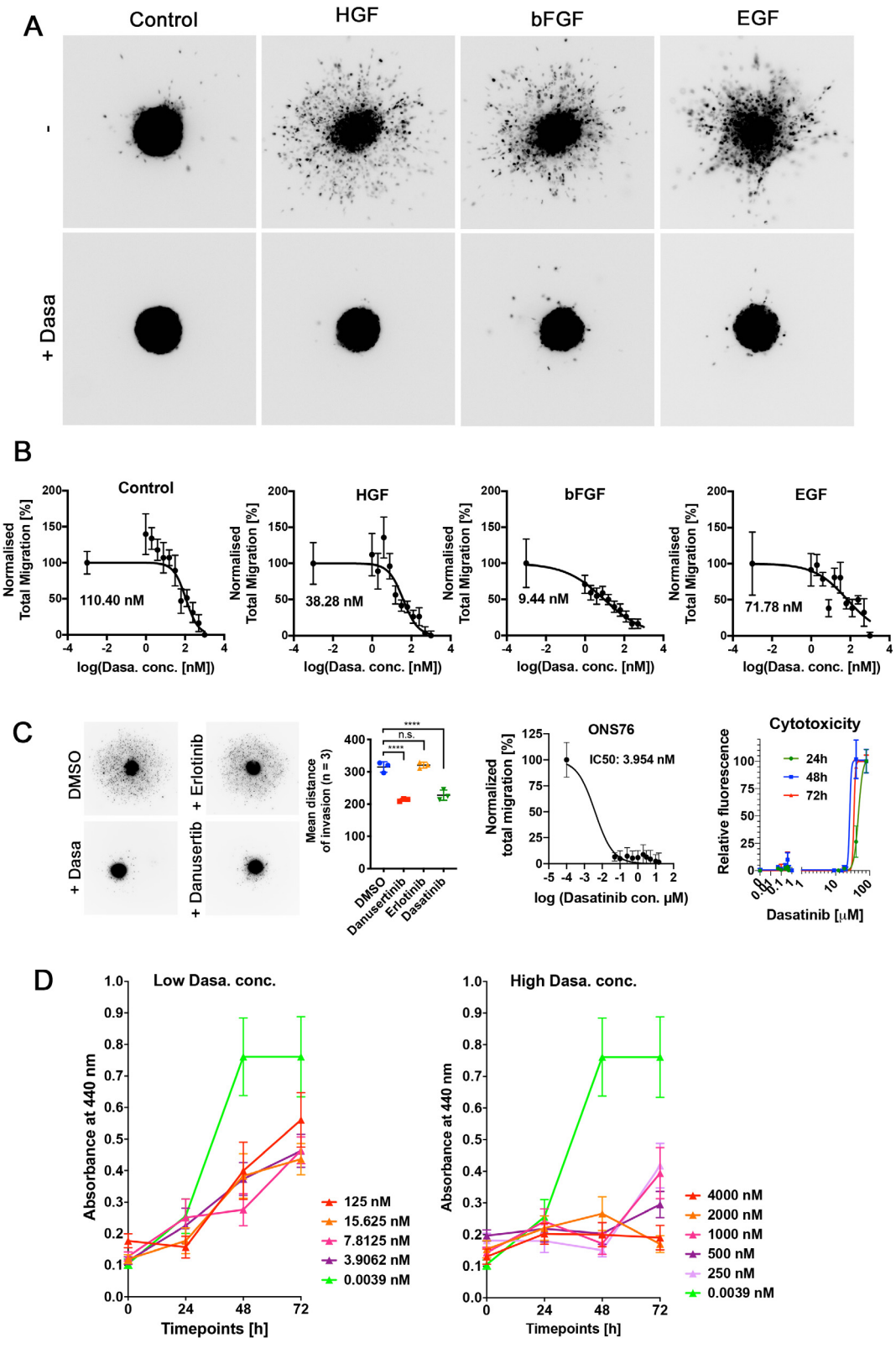

Fig. 2. Dasatinib blocks growth factor-induced collagen I invasion at nanomolar concentration. (A) Representative images of spheroid invasion assay (SIA) after the treatment of DAOY cell spheroids with growth factors only (top row) and in combination with dasatinib (3 µM, bottom row) for 24 h. (B) IC_{50} curves of dasatinib dose response effect on growth factor-induced collagen I invasion in DAOY cells. IC_{50}: Control = 110.40 nM, bFGF = 9.44 nM, EGF = 71.78 nM, HGF = 38.28 nM. (C) Impact of Dasatinib, Danusertib or Erlotinib, all at 3 µM, on collagen I invasion of the spontaneously invading SHH line ONS-76. *Left:* Representative images and corresponding quantification of triplicate measurements of mean distance of invasion. *Middle:* IC_{50} curve of dasatinib dose response effect on distance of invasion from collagen I-embedded ONS-76 spheroids. *Right:* CellTox green assay with ONS-76 tumor spheroids exposed to increasing concentrations of dasatinib. (D) WST assay to assess effect of increasing concentrations of dasatinib on DAOY cell proliferation and viability. Comparison of low (0.0039–125 nM, left graph) and high (250–4000 nM, right graph) concentrations of dasatinib on DAOY cells cultured in complete medium. The cells treated with 0.0039 nM of dasatinib were used as control condition (light green line).

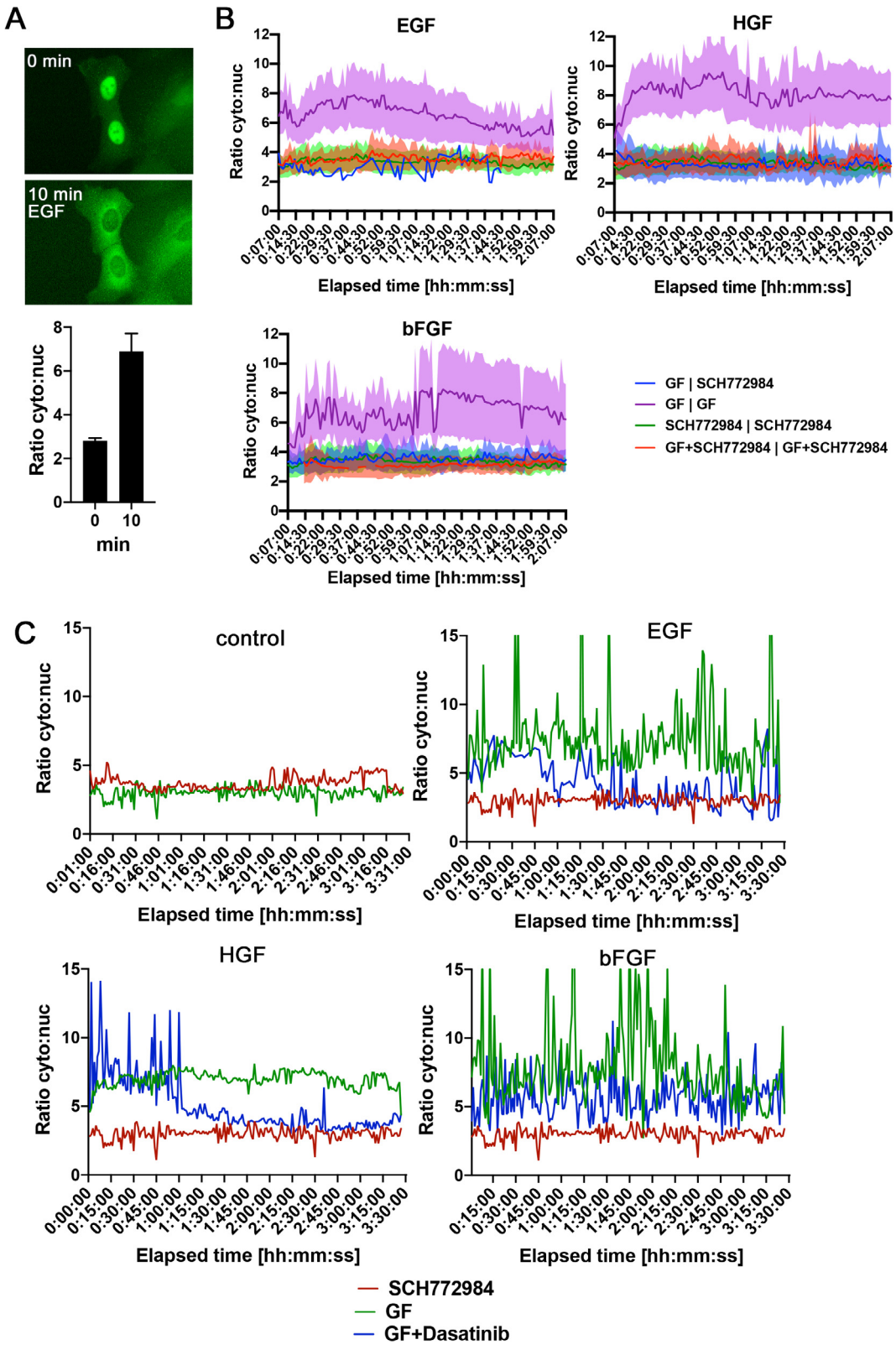

Fig. 3. Fast induction of SKARS translocation upon growth factor treatment. (A) Representative microscopy images of DAOY-ESKARS cells at timepoint 0 and 10 min post treatment with growth factors (top) and quantification of the ERK1/2 activity depicted as ratio of cytoplasmic fluorescence intensity to nuclear fluorescence intensity (bottom). (B) Quantification of real-time ERK1/2 activity measurements. The graphs show the measurement of the nuclear ERK1/2 activity as ratio of cytoplasmic:nuclear ESKARS after GF wash-out followed by treatment with either 1 μM ERK1/2 inhibitor SCH772984 (GF I SCH772984) or GF (GF I GF), or GF plus SCH772984 (GF + SCH772984 I GF + SCH772984) GF concentrations used: EGF (30 ng/ml), HGF (20 ng/ml) and bFGF (100 ng/ml). Dark lines: average, light-colored adjacent area: 95% confidence intervals. (C) Quantification of ERK1/2 sensor activation upon treatment with SCH772984 (baseline), with growth factors (GF) and with growth factors combined with 250 nM dasatinib (GF + dasatinib).

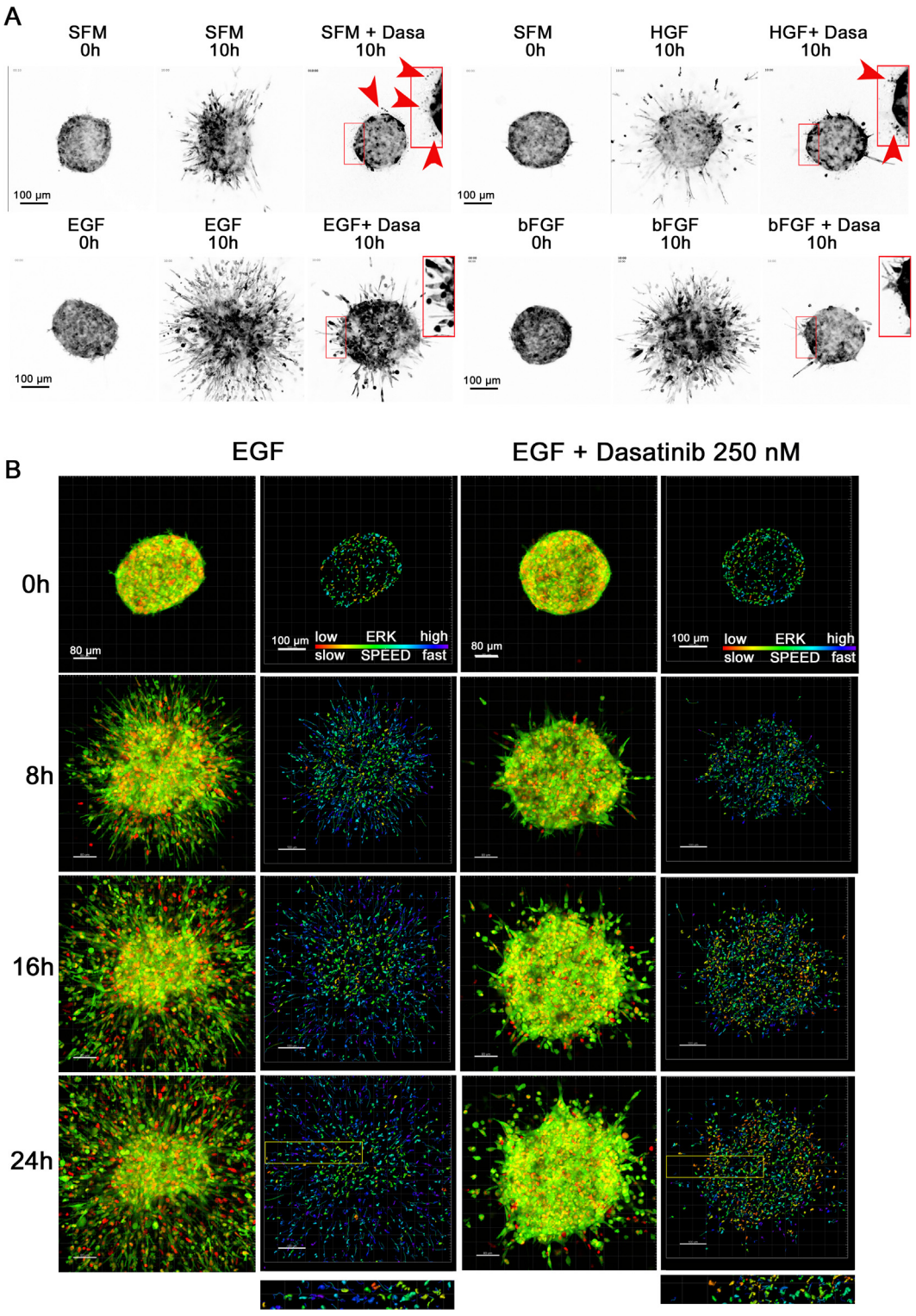

Fig. 4. Increased ERK1/2 activity in rapidly invading cells. (A) Inverted gray scale images of mClover fluorescence of collagen I-invading DAOY-ESKARS cells under growth factor treatments as indicated and without or with 250 nM dasatinib. Time points T0 h and T10 h are shown. Red squares indicate edges of spheroids and 2× magnifications thereof under dasatinib treatment for 10 h. (B) Snapshots of time-lapse imaging of EGF-induced collagen I invasion of DAOY-ESKARS cells in the absence of and presence of 250 nM dasatinib (M8 and M9). The left columns of each condition display still images of the overlaid green (mClover SKARS) and red (mCherry-nuc-9) channels at T0, T8, T16 and T24h. The right columns show the corresponding intensity measurements and analysis. The mean intensities are visualized in a scale from 0 to 250 and color-coded from red (low ERK1/2 activity) to blue (high ERK1/2 activity). The speed of the cells is visualized by dragon tails in a scale from 0 to 0.03 µm/s color-coded also from red (slow) to blue (fast). Scale bars microscopy pictures: 80 µm, scale bars analysis pictures: 100 µm. The area in the yellow boxes is magnified below the lowest speed vector panels for better visualization.

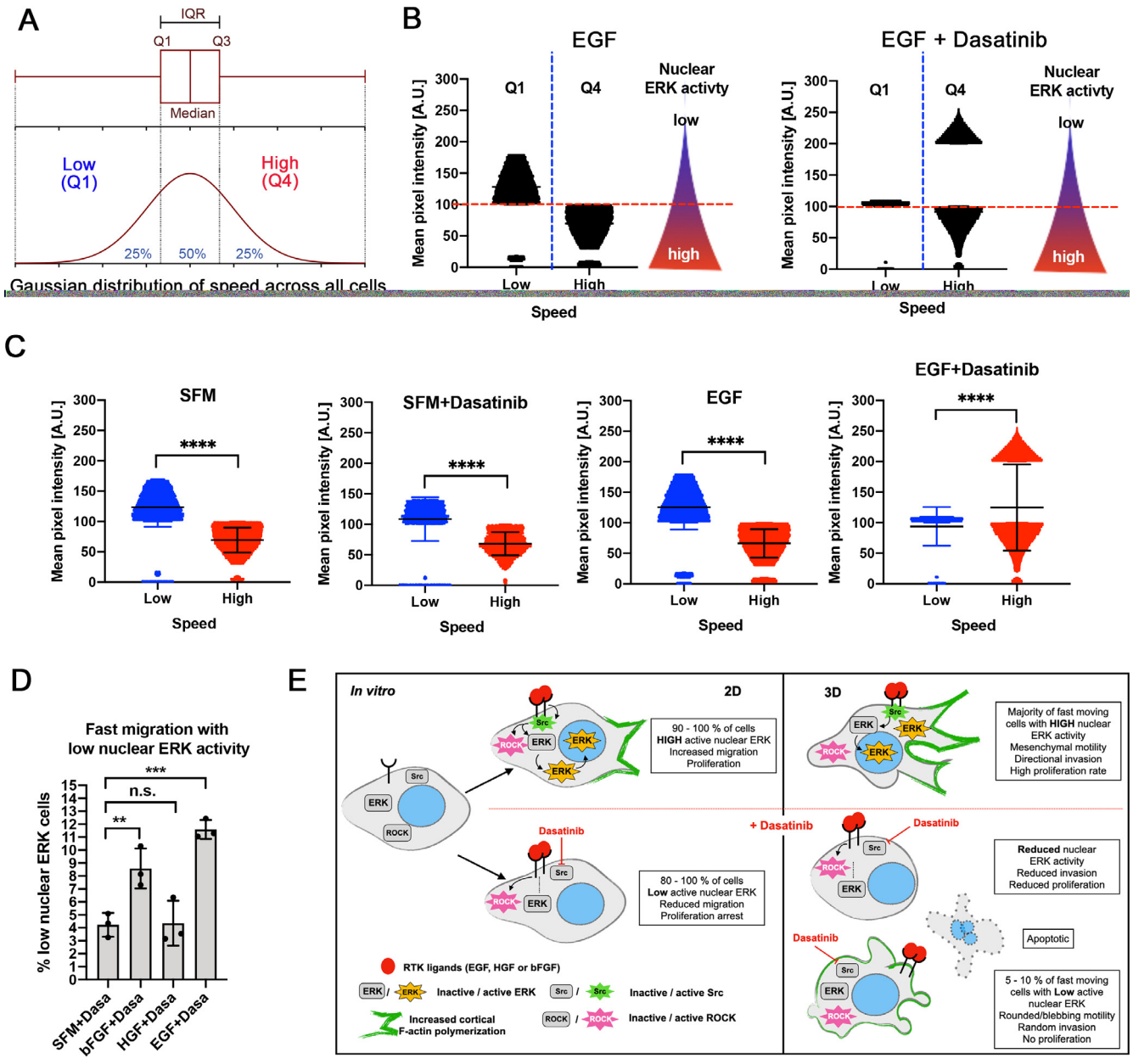

Fig. 5. High nuclear ERK1/2 correlates with high speed of migration. (A) The speed distribution across all cells measured is normally distributed. The resulting Gaussian distribution curve can be separated in three phases, low quartile (Q1), median quartile (Inter Quartile Range, IQR) and high quartile (Q4). (B) The mean pixel intensities (ESKARS fluorescence) in the nuclei of Q1 and Q4 cells treated −/+ 30 ng/ml EGF and −/+ 250 nM dasatinib were collected and plotted against speed. High mean pixel intensities indicate low nuclear ERK1/2 activity, low mean pixel intensities high nuclear ERK1/2 activity. (C) Mean pixel intensities in low (Q1, blue) and high (Q4, red) speed cells compared between unstimulated, EGF-stimulated and EGF −/+ dasatinib treatment. (D) Quantification of the percentage of dasatinib-treated cells with low nuclear ERK activity detected in the high-speed quartile (Q4). (E) Schematic summary of dasatinib effect on ERK1/2 activity and motility mode in 2D (tissue culture dishes, slides) and in 3D (inside collagen I matrices). The indicated effect of dasatinib on SRC kinases is based on literature information.

causes a subset of cells with low nuclear ERK1/2 activity to migrate rapidly in a rounded motility mode (Fig. 5E). This suggests that dasatinib treatment in the presence of activated growth factor receptors can promote the activation of an alternative cell migration program in MB cells.

Dasatinib only partially represses EGF-induced tumor cell expansion ex vivo

To explore the consequence of dasatinib treatment on tumor growth and tissue infiltration, we assessed the impact of dasatinib treatment on tumor expansion in organotypic cerebellum slice culture, which can be significantly increased by EGF treatment [32]. We confirmed that EGF treatment of cerebellar slices co-cultured with MB cells causes a marked expansion of the tumor cells compared to control and results in massive invasion of the tissue surrounding the spheroid (Fig. 6A). We also observed a considerable increase in EDU-positive nuclei after EGF stimulation, suggesting that EGF stimulation affects both proliferation and invasion. Co-treatment with dasatinib caused only a small reduction of tumor cell invasion distance (Fig. 6A, S5). However, we observed a considerable reduction in EDU-positive nuclei in the tumor cells, suggesting that dasatinib caused

complete repression of tumor cell proliferation after five days of treatment (Fig. 6A, S5). In addition, closer inspection of the cells at the invasion front revealed alterations in actin cytoskeleton morphology. Control and EGF-treated cells displayed filamentous protrusions at the cell edges facing the tissue environment (Fig. 6B, arrowheads). Dasatinib treatment in the absence of EGF completely abrogated these structures. Instead, we observed occasional bleb-like membrane extensions on cells near the invasion front. Co-stimulation of slices with EGF and dasatinib partially rescued filopodia formation compared to dasatinib treatment alone. Thus, although dasatinib treatment represses EGF-induced proliferation, it only partially represses EGF-induced tissue invasion of MB tumor cells. The reduction of filamentous F-actin assemblies in the cortex of the invading cells suggests that dasatinib treatment in the presence of activated growth factor receptors may shift the cell migration phenotype in a subset of cells from mesenchymal to rounded motility mode in a tissue context as well.

ROCK inhibition is necessary for complete repression of EGF-induced collagen I invasion

Rounded motility in cells treated with EGF and dasatinib indicated the implication of Rho-Kinase (ROCK) in invasion control as was previously shown for other invasive cancers *in vitro* and *in vivo* [33–35]. ROCK activation by TGF-Þ represses F-actin-rich filamentous protrusion formation in MB *cells in vitro* and *ex vivo*, which can be reverted by treating the cells with the ROCK inhibitor H-1152 [25]. H-1152 treatment of unstimulated DAOY cells in collagen I gels causes a massive increase in filamentous protrusions, which is in strong contrast to the complete repression of filamentous protrusions in dasatinib-treated cells (Fig. 7A, S6). The inhibition of SRC kinases by dasatinib causes membrane blebbing and mesenchymal to amoeboid transition in melanoma cells embedded in collagen I matrices [36]. We therefore tested whether rounded motility observed in EGF-stimulated dasatinib-treated cells is prevented by ROCK inhibition with H-1152. We found that dasatinib and H-1152 co-treatment of EGF-stimulated DAOY cells reduced collagen I invasion below levels measured for dasatinib treatment alone (Fig. 7B), suggesting that the inhibition of both the SRC- and the ROCK-driven motility modes is necessary for maximal repression of EGF-driven invasiveness. Consistently, co-treatment of EGF-stimulated cells with dasatinib and H-1152 caused complete disruption of F-actin structures and resulted in a disorganized actin cytoskeleton (Fig. 7B). These data indicate that combined inhibition of SRC-Rac and Rho-ROCK-driven F-actin polymerization is necessary to prevent EGF-induced migration of MB cells in 3D collagen I gels.

Discussion

In this study, we identified dasatinib as an effective inhibitor of growth factor induced collagen I invasion. Repression of invasion by dasatinib is associated with a marked reduction of nuclear ERK1/2 activity. In growth factor-stimulated control cells, nuclear ERK1/2 activity is increased within minutes, remains elevated for up to three hours and correlates positively with speed of migration. Dasatinib treatment does not completely block EGF-induced invasion and we observed cells with a rounded, blebbing morphology and low nuclear ERK1/2 activity invading collagen gels. Co-inhibition of Rho kinase ROCK is necessary for invasion inhibition of these cells. Together, our data indicate that dasatinib is an effective inhibitor of MAP kinase activation and cell migration downstream of growth factor stimulation. However, its therapeutic potential needs careful evaluation due to the onset of evading cells with a remarkable migratory potential that may need to be addressed with an inhibitor that specifically targets cell contractility and rounded motility.

Cox regression and gene set enrichment analysis point towards a key role of receptor tyrosine kinase-MAPK-ERK1/2 activation in the onset and progression of MB, in particular of SHH, Gr3 and Gr4 MB [5]. Our data revealed that growth factor stimulation results in acute nuclear ERK1/2 activation within minutes, which persists for at least two hours, similar to what had been previously described for EGF-stimulated ERK1/2-FRET biosensor activation [37]. Thus, unlike oncogenic activation of MAPK by mutant KRAS or BRAF, where feedback repression of ERK1/2 by the dual-specific phosphatase 4 (DUSP4) prevents sustained nuclear ERK1/2 activity [38], growth factor-stimulated ERK1/2 activity remains high in DAOY cells. Concomitant treatment with dasatinib reduces nuclear ERK1/2 activity to baseline within one hour in cells stimulated with EGF or HGF. Interestingly, in cells stimulated with bFGF, dasatinib treatment did not lead to a complete repression of nuclear ERK1/2 activity, suggesting a different regulation of nuclear ERK1/2 activation downstream of EGF and HGF compared to bFGF. One possibility is an altered de-repression of the ERK1/2 inhibitor DUSP4 by the polycomb group protein B lymphoma Mo-MLV insertion region 1 homolog (BMI), which promotes increased ERK1/2 activation and proliferation signaling in Gr4 MB [10]. BMI1 expression is up-regulated by bFGF-FGFR signaling in DAOY and the Gr3 MB line HD-MB03 [39], which may explain incomplete dasatinib repression of nuclear ERK1/2 activity through a BMI1-DUSP4-dependent mechanism.

Despite complete reduction of proliferation, we observed no effect of dasatinib on viability of cells growing in the presence of 10% serum. However, reduction of the serum concentration to less than 2%, as for example in the SIA, led to the appearance of debris around the spheroids. This suggests that serum rescues the cells from undergoing cell death induced by dasatinib. Cells are also rescued when stimulated with EGF but not when stimulated with HGF or bFGF, indicating that either the signal strength emanating from EGFRs or downstream effectors differ from those originating from c-Met or FGFR.

Dasatinib treatment of MB cells migrating in 2D on collagen-coated coverslips causes a rounded phenotype and partial detachment. This is most likely due to dasatinib inhibition of SRC family kinases, which are necessary for focal adhesion formation and turnover [36]. Similarly, dasatinib treatment of cells invading collagen I gels, a soft matrix triggering mesenchymal, integrin-dependent migration of DAOY cells [40], caused de-adhesion and cell rounding in other human tumor cells [36]. The process of migration associated with cell rounding and blebbing in response to de-adhesion and repression of pericellular proteolytic activity was referred to as mesenchymal to amoeboid transition (MAT) [41,42]. Dasatinib treatment of MB cells invading the brain tissue also results in cell rounding, the loss of F-actin-rich filamentous protrusions and bleb formation. Unlike in 2D, the formation of filamentous protrusions is partially rescued by EGF treatment, suggesting that the microenvironment of the brain tissue provides additional cues favoring filopodia formation. In collagen I matrix, where the ectopic growth factor and integrin activation provide the migration cues, EGF stimulation of dasatinib-treated cells causes a partial rescue of migration in a subset of cells, which migrate in a rounded, blebbing mode. We explain this by the fact that integrin-mediated adhesion signaling, which depends on SRC kinase activity [43], is lost in dasatinib-treated cells. A consequence of de-adhesion is the disruption and re-organization of the cortical action cytoskeleton and cell rounding, which are both necessary for blebbing motility [34,35]. Consistent with this possibility is our finding that blockade of cell rounding and blebbing by the Rho-kinase ROCK inhibitor H-1152 also repressed migration of this subset of cells. In EGFRwt/EGFRVIII glioblastoma multiforme tumor cells, a similar compensatory migration mechanism induced by dasatinib treatment was described recently, where the repression of ectopic activation of SRC kinases increased cell velocity [44]. In addition to the direct effect of EGF and dasatinib on the tumor cells, both treatments

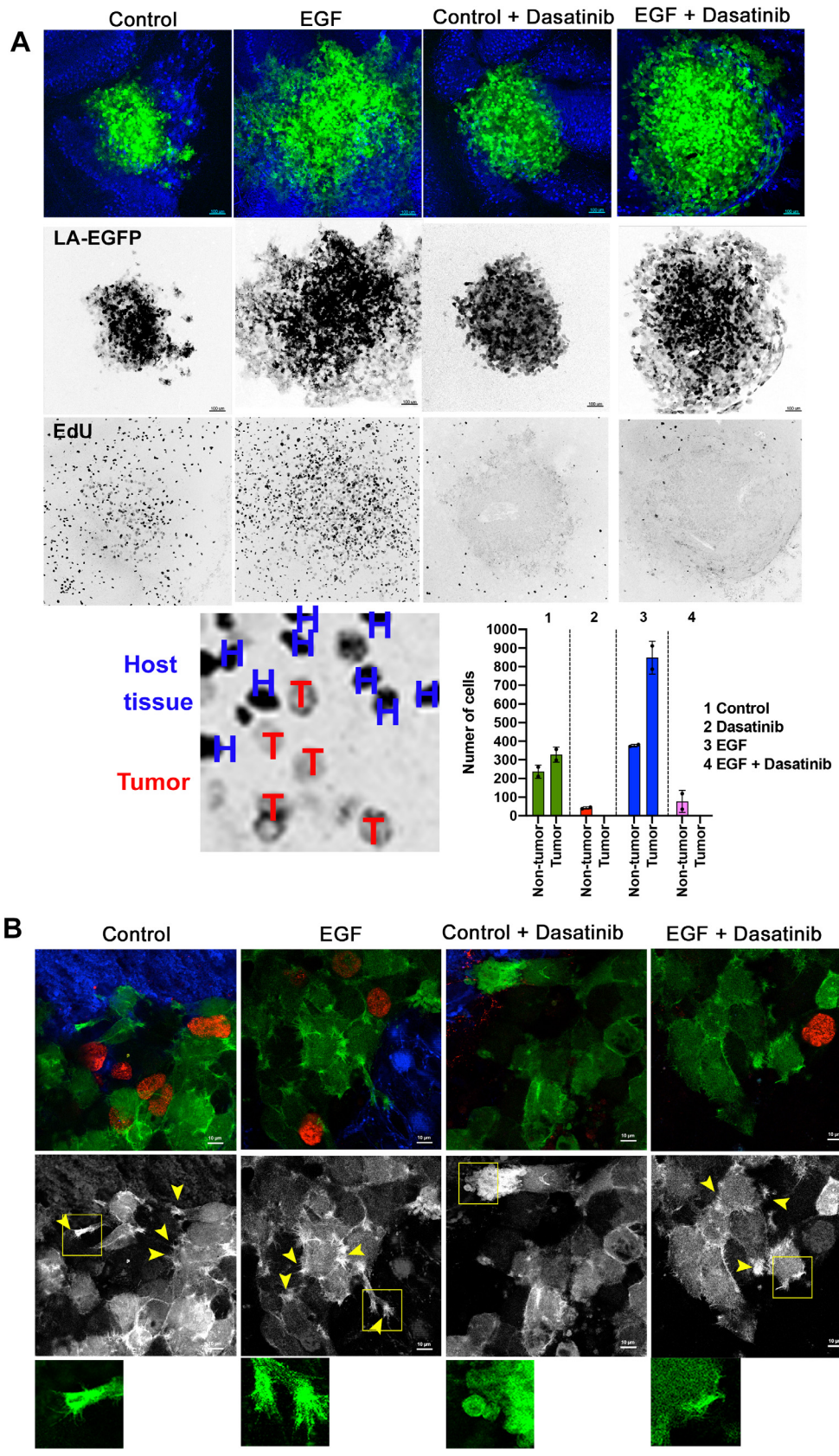

Fig. 6. Dasatinib causes only incomplete blockade of EGF-induced tissue invasion. (A) *Top:* Maximum intensity projections (MIP) of confocal sections of OCSC with implanted DAOY tumor cell spheroids. Treatments as indicated. Green: LA-EGFP, blue: Purkinje cells. *Middle:* Inverted gray scale images of MIP of LA-EGFP channel, *lower:* Inverted gray scale images of MIP of EDU staining. Scale bar corresponds to 100 µm. Magnification shows inverted gray scale images of EDU-positive nuclei of host tissue (H) and tumor cells (T). Bar diagram shows mean and standard deviation (SD) of EDU-positive nuclei in non-tumor and tumor cells. $N = 2$ experiments. (B) Magnification of invasion front of tumors shown in (A). *Upper:* Three color overlay of maximum intensity projection. Green: LA-EGFP, blue: Purkinje cells, red: EDU-positive tumor cell nuclei. *Middle:* Gray scale images of LA-EGFP channel. Arrowheads point to filamentous protrusions. Boxed areas are magnified 2× in bottom images. Scale bar corresponds to 10 µm.

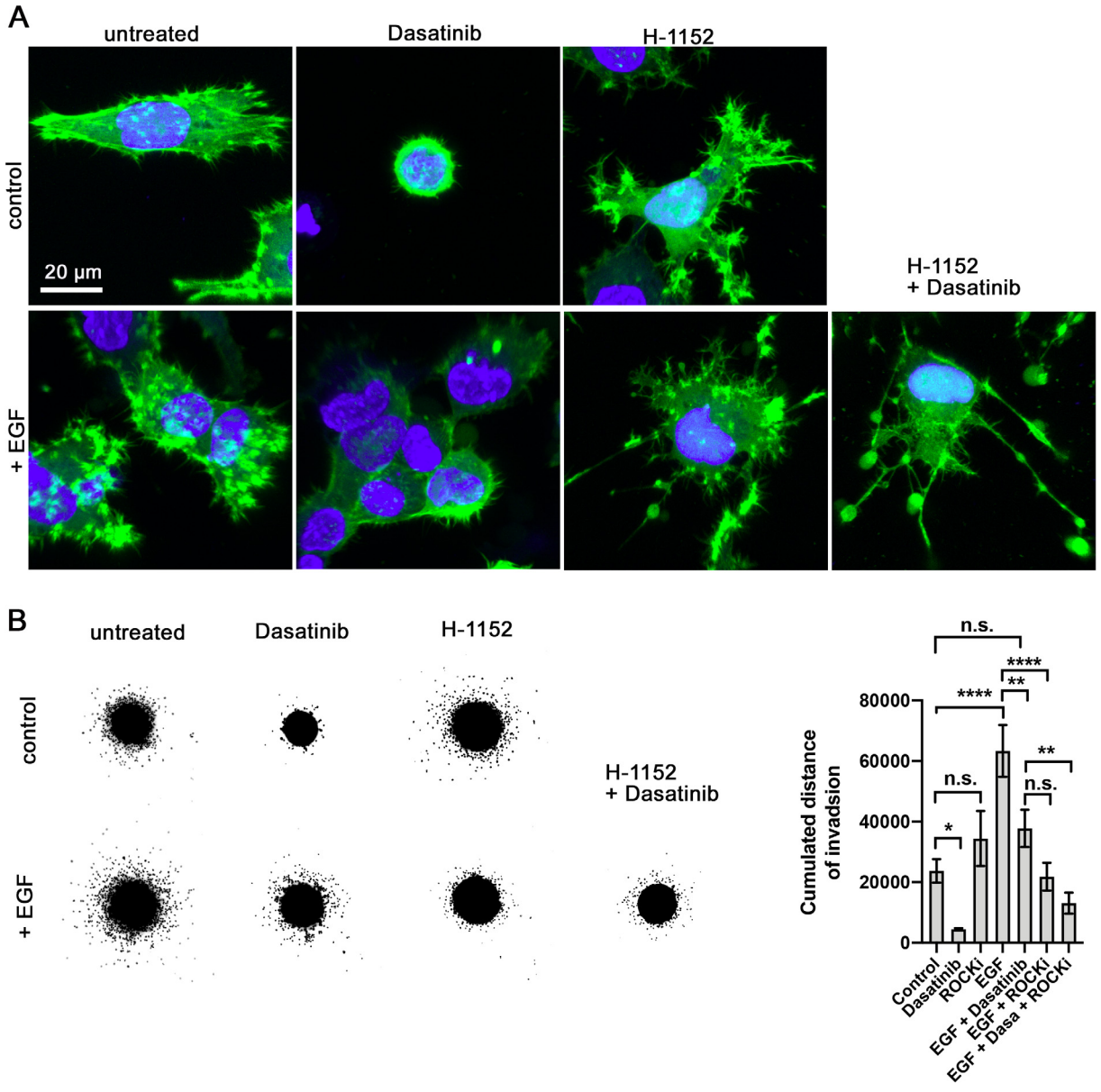

Fig. 7. Rho-kinase ROCK inhibition prevents rounded motility. (A) Maximum intensity projection of stack of confocal microscopy images of individual cells. Green: LA-EGFP, blue: Hoechst 33342. (B) *Left:* Representative inverted gray scale images of SIA of DAOY cells treated as indicated. *Right:* Mean and standard deviation of triplicate measurements of SIA shown on the left.

may also affect the tumor cell behavior indirectly via the modulation of the microenvironment. One indication for EGF-dependent alterations in the microenvironment is the increase in EDU-positive non-tumor cells in the cerebellar slices.

The delivery of targeted therapies across the blood brain barrier (BBB) challenges clinical translation of promising drugs. Indeed, the brain penetration of dasatinib is poor, with a CSF:plasma ratio ranging from 0.05 to 0.28. Nevertheless, dasatinib appears to be more potent against CNS tumors than imatinib, possibly due to a much greater potency of dasatinib and the large fraction of unbound drug [45]. Hence, coupling of dasatinib to α_v integrin-directed cRGD silica nanoparticles, which facilitates drug passage across the partially disrupted BBB in a murine GBM model, may be necessary for increasing the accumulation, retention, and diffusion of the drug [46]. An alternative strategy is convection-enhanced delivery of dasatinib in combination with the ABC transporter inhibitor tariquidar and dexamethasone, which enhanced tumor cell apoptosis and survival in a mouse model of H3.3K27M mutant diffuse intrinsic pons glioma [47]. However, the effect of dasatinib to promote a mesenchymal to amoeboid transition in a subset of cells calls for cautious monitoring of therapeutic benefits, in particular with respect to the consequence of drug treatment on local infiltration at primary and metastatic sites.

Acknowledgements

The authors thank Dr. Serge Pelet, University of Lausanne for sharing the ERK-SKARS construct. Imaging and image analysis and quantification was performed with the support of the Centre for Microscopy and Image Analysis of the University of ZÏrich.

Funding

This work was supported by the Stiftung fÎr Wissenschaftliche Forschung (grant STWF-17-03), Childhood Cancer Switzerland, the Swiss National Science Foundation (grant SNF_31003A_165860/1) and the Swiss Cancer League (grant KLS-3834-02-2016).

Appendix A. Supplementary data

Supplementary data to this article can be found online at https://doi.org/10.1016/j.neo.2020.07.006.

References

1. MacDonald TJ, Brown KM, LaFleur B, Peterson K, Lawlor C, Chen Y, Packer P, Cogen P, Stephan DA. Expression profiling of medulloblastoma: PDGFRA and the RAS/MAPK pathway as therapeutic targets for metastatic disease. *Nat Genet* 2001;**29**:143–52.
2. Liang L, Coudiere-Morrison L, Tatari N, Stromecki M, Fresnoza A, Porter CJ, Del Bigio MR, Hawkins C, Chan JA, Ryken TC, Taylor MD, Ramaswamy V, Werbowetski-Ogilvie TE. CD271(+) Cells are diagnostic and prognostic and exhibit elevated MAPK activity in SHH medulloblastoma. *Cancer Res* 2018;**78**:4745–59.
3. da Cunha Jaeger M, Ghisleni EC, Cardoso PS, Siniglaglia M, Falcon T, Brunetto AT, Brunetto AL, de Farias CB, Taylor MD, NÎr C, Ramaswamy V, Roesler R. HDAC and MAPK/ERK inhibitors cooperate to reduce viability and stemness in medulloblastoma. *J Mol Neurosci* 2020. https://doi.org/10.1007/s12031-020-01505-y.
4. Zhao X, Ponomaryov T, Ornell KJ, Zhou P, Dabral SK, Pak E, Li W, Atwood RJ, Whitson RJ, Chang ALS, Li J, Oro AE, Chan JA, Kelleher JF, Segal RA. RAS/MAPK activation drives resistance to Smo inhibition, metastasis, and tumor evolution in Shh pathway-dependent tumors. *Cancer Res* 2015;**75**:3623–35.
5. Park AK, Lee J-Y, Cheong H, Ramaswamy V, Park S-H, Kool M, Phi JH, Choi SA, Cavalli F, Taylor MD, Kim S-K. Subgroup-specific prognostic signaling and metabolic pathways in pediatric medulloblastoma. *BMC Cancer* 2019;**19**:571.
6. Meco D, Servidei T, Riccardi A, Ferlini C, Cusano G, Zannoni GF, Giangaspero F, Riccardi R. Antitumor effect in medulloblastoma cells by gefitinib: ectopic HER2 overexpression enhances gefitinib effects in vivo. *Neurol Oncol* 2009;**11**:250–9.
7. Cavalli FMG et al. Intertumoral heterogeneity within medulloblastoma subgroups. *Cancer Cell* 2017;**31**:737–754.e6.
8. Schwalbe EC, Lindsey JC, Nakjang S, Crosier S, Smith AJ, Hicks D, Rafiee G, Hill RM, Iliasova A, Stone T, Pizer B, Michalski A, Joshi A, Wharton SB, Jacques TS, Bailey S, Williamson D, Clifford SC. Novel molecular subgroups for clinical classification and outcome prediction in childhood medulloblastoma: a cohort study. *Lancet Oncol* 2017;1–14. https://doi.org/10.1016/S1470-2045(17)30243-7.
9. Hovestadt V, Ayrault O, Swartling FJ, Robinson GW, Pfister SM, Northcott PA. Medulloblastomics revisited: biological and clinical insights from thousands of patients. *Nat Rev Cancer* 2020;**20**:42–56.
10. Badodi S, Dubuc A, Zhang X, Rosser G, da Cunha Jaeger M, Kameda-Smith AS, Morrissy AS, Guilhamon P, Suetterlin P, Li X-N, Guglielmi L, Merve A, Farooq H, Lupien M, Singh SK, Basson MA, Taylor MD, Marino S. Convergence of BMI1 and CHD7 on ERK signaling in medulloblastoma. *Cell Rep* 2017;**21**:2772–84.
11. Maik-Rachline G, Hacohen-Lev-Ran A, Seger R. Nuclear ERK: mechanism of translocation, substrates, and role in cancer. *Int J Mol Sci* 2019;**20**.
12. Rubinfeld H, Hanoch T, Seger R. Identification of a cytoplasmic-retention sequence in ERK2. *J Biol Chem* 1999;**274**:30349–52.
13. Plotnikov A, Chuderland D, Karamansha Y, Livnah O, Seger R. Nuclear ERK translocation is mediated by protein kinase CK2 and accelerated by autophosphorylation. *Cell Physiol Biochem* 2019;**53**:366–87.
14. Chuderland D, Konson A, Seger R. Identification and characterization of a general nuclear translocation signal in signaling proteins. *Mol Cell* 2008;**31**:850–61.
15. de la Cova C, Townley R, Regot S, Greenwald I. A real-time biosensor for ERK activity reveals signaling dynamics during C. elegans cell fate specification. *Dev Cell* 2017;**42**:542–553.e4.
16. Ma M, Bordignon P, Dotto GP, Pelet SP. Visualizing cellular heterogeneity by quantifying the dynamics of MAPK activity in live mammalian cells with synthetic fluorescent biosensors. *biorxiv.org* 2019. https://doi.org/10.1101/760652.
17. Samatar AA, Poulikakos PI. Targeting RAS-ERK signalling in cancer: promises and challenges. *Nat Rev Drug Disc* 2014;**13**:928–42.
18. Day EK, Sosale NG, Xiao A, Zhong Q, Purow B, Lazzara MJ. Glioblastoma cell resistance to EGFR and MET inhibition can be overcome via blockade of FGFR-SPRY2 bypass signaling. *Cell Rep* 2020;**30**:3383–3396.e7.
19. Kitai H, Ebi H. Key roles of EMT for adaptive resistance to MEK inhibitor in KRAS mutant lung cancer. *Small GTPases* 2017;**8**:172–6.
20. Shah NP, Tran C, Lee FY, Chen P, Norris D, Sawyers CL. Overriding imatinib resistance with a novel ABL kinase inhibitor. *Science (80-.)* 2004;**305**:399–401.
21. Forget A et al. Aberrant ERBB4-SRC signaling as a hallmark of group 4 medulloblastoma revealed by integrative phosphoproteomic profiling. *Cancer Cell* 2018;**34**:379–395.e7.
22. Faria CC et al. Foretinib is effective therapy for metastatic sonic hedgehog medulloblastoma. *Cancer Res* 2015;**75**:134–46.
23. Guessous F, Yang Y, Johnson E, Marcinkiewicz L, Smith M, Zhang Y, Kofman D, Schiff D, Christensen J, Abounader R. Cooperation between c-Met and focal adhesion kinase family members in medulloblastoma and implications for therapy. *Mol Cancer Ther* 2012;**11**:288–97.
24. Santhana Kumar K, Tripolitsioti D, Ma M, GrÌhlert J, Egli KB, Fiaschetti G, Shalaby T, Grotzer MA, Baumgartner M. The Ser/Thr kinase MAP4K4 drives c-Met-induced motility and invasiveness in a cell-based model of SHH medulloblastoma. *Springerplus* 2015;**4**.
25. Santhana Kumar K, Neve A, Guerreiro Stucklin AS, Kuzan-Fischer CM, Rushing EJ, Taylor MD, Tripolitsioti D, Behrmann L, Kirschenbaum D, Grotzer MA, Baumgartner M. TGF-β determines the pro-migratory potential of bFGF signaling in medulloblastoma. *Cell Rep* 2018;**23**:3798–3812.e8.
26. Petersen W, Liu J, Yuan L, Zhang H, Schneiderjan M, Cho Y-J, Macdonald TJ. Dasatinib suppression of medulloblastoma survival and migration is markedly enhanced by combining treatment with the aurora kinase inhibitor AT9283. *Cancer Lett* 2014;**354**:68–76.
27. Wei J, Ma L, Li C, Pierson CR, Finlay JL, Lin J. Targeting upstream kinases of STAT3 in human medulloblastoma cells. *Curr Cancer Drug Targets* 2019;**19**:571–82.
28. Fiaschetti G, Schroeder C, Castelletti D, Arcaro A, Westermann F, Baumgartner M, Shalaby T, Grotzer MA. NOTCH ligands JAG1 and JAG2 as critical pro-survival factors in childhood medulloblastoma. *Acta Neuropathol Commun* 2014;**2**.
29. Yamada M, Shimizu K, Tamura K, Okamoto Y, Matsui Y, Moriuchi S, Park K, Mabuchi E, Yamamoto K, Hayakawa T. Establishment and biological characterization of human medulloblastoma cell lines. *Brain Nerve* 1989;**41**:695–702.
30. Kumar KS, Pillong M, Kunze J, Burghardt I, Weller M, Grotzer MA, Schneider G, Baumgartner M. Computer-assisted quantification of motile and invasive capabilities of cancer cells. *Sci Rep* 2015;**5**.
31. Schindelin J, Arganda-Carreras I, Frise E, Kaynig V, Longair M, Pietzsch T, Preibisch S, Rueden C, Saalfeld S, Schmid B, Tinevez JY, White DJ, Hartenstein V, Eliceiri K, Tomancak P, Cardona A. Fiji: An open-source platform for biological-image analysis. *Nat Methods* 2012;**9**:676–82.
32. Neve A, Kumar KS, Tripolitsioti D, Grotzer MA, Baumgartner M. Investigation of brain tissue infiltration by medulloblastoma cells in an ex vivo model. *Sci Rep* 2017;**7**.
33. Wyckoff JB, Pinner SE, Gschmeissner S, Condeelis JS, Sahai E. ROCK- and myosin-dependent matrix deformation enables protease-independent tumor-cell invasion in vivo. *Curr Biol* 2006;**16**:1515–23.
34. Fackler OT, Grosse R. Cell motility through plasma membrane blebbing. *J Cell Biol* 2008;**181**:879–84.
35. Charras G, Paluch E. Blebs lead the way: how to migrate without lamellipodia. *Nat Rev Mol Cell Biol* 2008;**9**:730–6.
36. Logue JS, Cartagena-Rivera AX, Chadwick RS. C-SRC activity is differentially required by cancer cell motility modes. *Oncogene* 2018;**37**:2104–21.
37. BlÏthgen N. Signaling output: it's all about timing and feedbacks. *Mol Syst Biol* 2015;**11**:843.

38. Cagnol S, Rivard N. Oncogenic KRAS and BRAF activation of the MEK/ERK signaling pathway promotes expression of dual-specificity phosphatase 4 (DUSP4/MKP2) resulting in nuclear ERK1/2 inhibition. *Oncogene* 2013;**32**:564–76.
39. Neve A, Migliavacca J, Capdeville C, SchÎnholzer MT, Gries A, Ma M, Kumar M, Grotzer M, Baumgartner M. Crosstalk between SHH and FGFR signaling pathways controls tissue invasion in medulloblastoma. *Cancers (Basel)* 2019;**11**
40. Tripolitsioti D, Kumar KS, Neve A, Migliavacca J, Capdeville C, Rushing EJ, Ma M, Kijima N, Sharma A, Pruschy M, McComb S, Taylor MD, Grotzer M, Baumgartner M. MAP4K4 controlled integrin β1 activation and c-Met endocytosis are associated with invasive behavior of medulloblastoma cells. *Oncotarget* 2018;**9**.
41. Wolf K, Mazo I, Leung H, Engelke K, Von Andrian UH, Deryugina EI, Strongin AY, BrÎcker EB, Friedl P. Compensation mechanism in tumor cell migration: Mesenchymal-amoeboid transition after blocking of pericellular proteolysis. *J Cell Biol* 2003;**160**:267–77.
42. Sahai E, Marshall CJ. Differing modes for tumour cell invasion have distinct requirements for Rho/ROCK signalling and extracellular proteolysis. *Nat Cell Biol* 2003;**5**:711–9.
43. Hamidi H, Ivaska J. Every step of the way: integrins in cancer progression and metastasis. *Nat Rev Cancer* 2018;**18**:533–48.
44. Jubran MR, Rubinstein AM, Cojocari I, Adejumobi IA, Mogilevsky M, Tibi S, Sionov RV, Verreault M, Idbaih A, Karni R, Kravchenko-Balasha N. Dissecting the role of crosstalk between glioblastoma subpopulations in tumor cell spreading. *Oncogenesis* 2020;**9**:11.
45. Korashy HM, Rahman AFMM, Kassem MG. Chapter Four – Dasatinib. In Profiles of Drug Substances, Excipients and Related Methodology (ed. Brittain, H. G.) pp. 2–551 (Academic Press, Elsevier).
46. Juthani R et al. Ultrasmall core-shell silica nanoparticles for precision drug delivery in a high-grade malignant brain tumor model. *Clin Cancer Res* 2020;**26**:147–58.
47. Tsvankin V, Hashizume R, Katagi H, Herndon JE, Lascola C, Venkatraman D, Picard D, Burrus B, Becher OJ, Thompson EM. ABC transporter inhibition plus dexamethasone enhances the efficacy of convection enhanced delivery in H3.3K27M mutant diffuse intrinsic pontine glioma. *Neurosurgery* 2019;**15**:88.